DOI 10.24425/aee.2026.6351

Theoretical analysis of the secondary circuit of an electric arc furnace under three-phase unbalance condition

WEIJIAN LI[1], YANG YANG[2], LONGHU CAO[2]✉

[1] *WISDRI Engineering & Research Incorporation Limited*
Wuhan 430070, China

[2] *Innovation Research Institute of Low Carbon Metallurgical Engineering, School of Materials and Energy*
Guangdong University of Technology
Guangzhou 510006, China

e-mail: ✉ *caolonghu1989@gdut.edu.cn*

(Received: 16.07.2026, revised: 19.10.2026)

Abstract: During electric arc furnace (EAF) smelting, three-phase load imbalance significantly affects electrical energy losses, temperature uniformity in the molten bath, and overall smelting efficiency. Therefore, based on the three-phase unbalanced circuit of the EAF, this paper establishes a mathematical calculation model for key parameters related to production stability, including: neutral point voltage, three-phase voltage unbalance degree, three-phase currents, arc length, negative-sequence current, and voltage unbalance degree at the point of common coupling (PCC). Simulation results based on a 120 t EAF indicate that an increase in the impedance unbalance degree leads to a corresponding rise in neutral point voltage and three-phase voltage unbalance degree, accompanied by a marked increase in inter-phase current disparity and current unbalance degree. Notably, as the impedance unbalance degree escalates from 10% to 30%, the three-phase arc length difference widens from 26 mm to 79 mm, the relative negative-sequence current climbs from 2.89% to 8.76%, and the unbalance degree of PCC voltage increases from 0.276% to 0.846%. The theoretical findings presented in this paper provide a foundation for balanced compensation and operational optimization of EAF power supply systems.

Key words: arc length, EAF, negative-sequence current, secondary circuit, unbalance degree

1. Introduction

As core electrical equipment in industries such as metallurgy and machinery manufacturing, the power supply circuit of an electric arc furnace (EAF) is mostly a high-power three-phase system. Three-phase balance is the foundation for ensuring stable equipment operation and improving

© 2026. The Author(s). This is an open-access article distributed under the terms of the Creative Commons Attribution-NonCommercial-NoDerivatives License (CC BY-NC-ND 4.0, https://creativecommons.org/licenses/by-nc-nd/4.0/), which permits use, distribution, and reproduction in any medium, provided that the Article is properly cited, the use is non-commercial, and no modifications or adaptations are made.

energy utilization efficiency [1–4]. However, during actual operation, affected by factors including electrode position fluctuations, uneven furnace charge distribution, impedance asymmetry, and nonlinear arc characteristics, the EAF power supply circuit is prone to three-phase unbalance. This leads to unequal amplitudes and phase shifts of three-phase voltage and current, which in turn causes problems such as disordered power distribution and excessive unbalance. Aliferov *et al*. [5] determined through theoretical analysis and modeling that three-phase impedance unbalance caused by structural asymmetry of the secondary circuit induces unequal magnitudes and phase shifts in three-phase voltages and currents, even under arc-symmetrical conditions. Kozyra *et al*. [6] indicated that, due to interphase interactions within the electrode control system, a change in the arc length of a single phase triggers unintended actual electrode movements in the remaining phases. From a control perspective, this consequently results in magnitude inequality and phase displacement of the three-phase voltages and currents.

Three-phase unbalance not only increases losses in power supply lines and transformers and reduces equipment service life, but also affects the smelting effect of electric arc furnaces (EAFs) due to uneven three-phase power distribution, leading to fluctuations in product quality, while simultaneously increasing the difficulty of power grid power quality management [7]. Yang *et al.* [8] found through multi-physics modeling that three-phase unbalance increases a transformer's total loss by approximately 17.31%, while exacerbating thermal stress and aging. Furthermore, reducing the load rate to 90% can lower the relative aging rate to about 20% of that under full load, thereby effectively extending the transformer's service life. Jagiela *et al*. [9] pointed out that voltage fluctuations induced by three-phase unbalance directly undermine arc stability. Since arc stability determines the uniformity of heat distribution inside the furnace, it further affects the melting and refining processes, ultimately leading to product quality fluctuations. Sivtsov *et al*. [10] demonstrated that short-circuit asymmetry and interphase power transfer caused by three-phase unbalance are the main causes of nonuniform charge melting in EAFs (with a power deficit of 1.2 MWh at the "dead" phase), thus confirming that uneven three-phase power distribution directly affects smelting performance. Shurygin [11] pointed out that nonuniform power distribution among the phases of an EAF reduces the active power component used to heat metal and slag, leading to a 7.4% increase in total electrical energy consumption and a 9% increase in electrode consumption. Babaei *et al*. [12] revealed a coupling dependency among the electrical quantities of three-phase arcs, whereby the voltage and current of each phase are functions of the electrical quantities of the other two phases. At present, research on EAF three-phase unbalance is mostly focused on unbalance suppression measures, and lacks systematic analysis of the internal relationship between three-phase voltage, three-phase current, three-phase power and three-phase unbalance degree under unbalanced conditions. Existing research cannot accurately quantify the coupling relationships between various parameters, nor can it provide accurate theoretical support for unbalance control and power supply system optimization.

Based on this, this paper focuses on the research and parametric modeling of three-phase unbalanced circuits in EAFs, aiming to investigate the variation characteristics of three-phase voltages and currents under unbalanced working conditions, reveal the inherent correlations between the three-phase unbalance degree and key electrical parameters, and establish a reasonable parameter calculation model. The proposed research not only advances the theoretical framework for unbalance analysis in EAF power supply circuits, but also provides a solid foundation for parameter optimization, unbalance forecasting, and unbalance remediation in practical engineering

applications. As such, it holds important theoretical value and practical engineering significance for improving the operational stability of EAFs, reducing energy consumption, and maintaining the power quality of the power grid.

2. Secondary circuit of EAF

During normal smelting operations in an EAF, the thermal energy required to heat the molten steel bath is primarily generated by resistive heating from the electric arcs formed at the electrode tips. Accordingly, the entire secondary power supply circuit mainly consists of impedance components including transformers, reactors, secondary cables, and electric arcs. Among these components, the reactor windings, secondary circuits, and electric arcs are connected to the three-phase system as individual single-phase units, while the primary and secondary windings of the transformer are connected in a delta configuration. The three-phase circuit schematic of the system investigated in this study is shown in Fig. 1, and the detailed definitions of all parameters in the figure are listed in Table 1.

Table 1. Parameters of three-phase circuit diagram of the EAF

Parameters	**Definition**	**Unit**
U_{12}	Line voltage between phase 1 and phase 2	V
U_{23}	Line voltage between phase 2 and phase 3	V
U_{31}	Line voltage between phase 3 and phase 1	V
I_1	Line current between phase 1 and phase 2	A
I_2	Line current between phase 2 and phase 3	A
I_3	Line current between phase 3 and phase 1	A
I_{D1}	Current of phase 1	A
I_{D2}	Current of phase 2	A
I_{D3}	Current of phase 3	A
r_{reactor}	Reactor resistance	Ω
x_{reactor}	Reactor reactance	Ω
$r_{\text{transformer}}$	Coil resistance of EAF transformer	Ω
$x_{\text{transformer}}$	Coil reactance of EAF transformer	Ω
r_{circuit}	Resistance of secondary circuit	Ω
x_{circuit}	Reactance of secondary circuit	Ω
r_{arc}	Resistance of electric arc	Ω

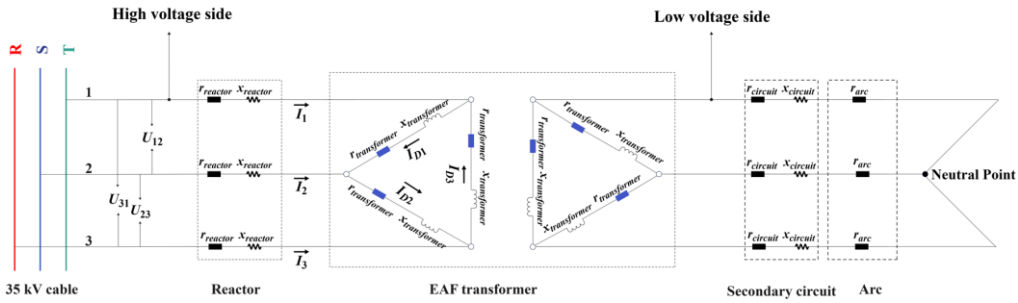


Fig. 1. Three-phase circuit diagram of the EAF

As shown in Fig. 1, the EAF transformer adopts a delta connection, which is inconvenient for the calculation of three-phase unbalanced circuits and requires equivalent conversion to a star connection. Meanwhile, during the EAF smelting process, multiple factors including fluctuations in molten steel level, uneven furnace charge distribution, electrode position fluctuations, loop impedance asymmetry, and the nonlinear characteristics of arcs make the EAF power supply circuit prone to three-phase unbalance. This unbalance causes unequal magnitudes of three-phase voltages and currents as well as phase shifts, and consequently leads to problems such as disordered power distribution and excessive unbalance degree. Therefore, to accurately calculate the three-phase unbalance degree during EAF smelting and establish the intrinsic relationship between three-phase voltage, three-phase current, three-phase power and the unbalance degree, this paper constructs an equivalent circuit diagram for EAF power supply under unbalanced conditions, as shown in Fig. 2.

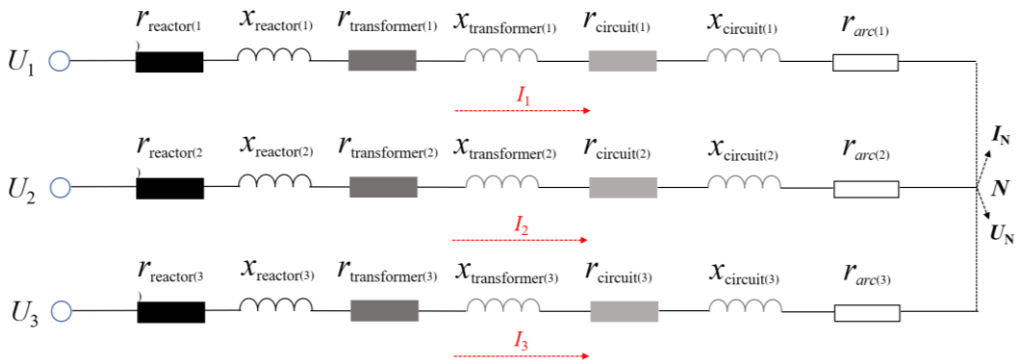


Fig. 2. Equivalent three-phase unbalanced power supply circuit

As can be seen from Fig. 1, the calculation formula for the total resistance r_1 of phase 1 in the power-supply circuit of the EAF is as follows:

$$r_1 = r_{\text{reactor1}} + r_{\text{transformer1}} + r_{\text{circuit1}} + r_{\text{arc1}} \tag{1}$$

and, the short-circuit reactance x_1 in phase 1 is:

$$x_1 = x_{\text{reactor1}} + x_{\text{transformer1}} + x_{\text{circuit1}}. \tag{2}$$

During the actual operation of the EAF, the calculation formula for the operating reactance x_{op1} of phase 1:

$$x_{\text{op1}} = k_1 \times (x_{\text{reactor1}} + x_{\text{transformer1}} + x_{\text{circuit1}}). \tag{3}$$

Similarly, the total resistance r_2 in phase 2 is:

$$r_2 = r_{\text{reactor2}} + r_{\text{transformer2}} + r_{\text{circuit2}} + r_{\text{arc2}} \tag{4}$$

and, the short-circuit reactance x_2 in phase 2 is:

$$x_2 = x_{\text{reactor2}} + x_{\text{transformer2}} + x_{\text{circuit2}}. \tag{5}$$

During the actual operation of the EAF, its operating reactance x_{op2} is:

$$x_{\text{op2}} = k_2 \times (x_{\text{reactor2}} + x_{\text{transformer2}} + x_{\text{circuit2}}). \tag{6}$$

The total resistance r_3 in phase 3 is:

$$r_3 = r_{\text{reactor3}} + r_{\text{transformer3}} + r_{\text{circuit3}} + r_{\text{arc3}} \tag{7}$$

and, the short-circuit reactance x_3 in phase 3 is:

$$x_3 = x_{\text{reactor3}} + x_{\text{transformer3}} + x_{\text{circuit3}}. \tag{8}$$

During the actual operation of the EAF, its operating reactance x_{op3} is:

$$x_{\text{op3}} = k_3 \times (x_{\text{reactor3}} + x_{\text{transformer3}} + x_{\text{circuit3}}). \tag{9}$$

Here, k_1, k_2 and k_3 are the operating reactance coefficients of the three phases in the power supply circuit of the EAF caused by harmonics.

3. Calculation of unbalanced secondary circuits

3.1. Impedance of the three phases

EAF smelting is a high-impact nonlinear load that often causes severe three-phase load asymmetry, voltage fluctuation and flicker, and harmonic injection into the power grid. It is also accompanied by low power factor and voltage distortion, which significantly degrades power quality. Research on three-phase unbalanced circuits of electric arc furnaces helps optimize power supply operation conditions, reduce smelting power consumption, alleviate grid impact and equipment overload, prevent electrical safety hazards, and provide a theoretical basis for the energy-saving, stable and safe operation of EAFs.

Based on the diagram of three-phase balanced circuit shown in Fig. 2, the impedance values Z_1, Z_2 and Z_3 for the three phases are derived.

The impedance of phase 1 in the power supply circuit:

$$Z_1 = r_1 + jx_{\text{op1}} = \sqrt{r_1^2 + x_{\text{op1}}^2}\angle\varphi_1, \quad \varphi_1 = \arctan\left(\frac{x_{\text{op1}}}{r_1}\right) \Omega. \tag{10}$$

The impedance of phase 2 in the power supply circuit:

$$Z_2 = r_2 + jx_2 = \sqrt{r_2^2 + x_{\text{op2}}^2}\angle\varphi_2, \quad \varphi_2 = \arctan\left(\frac{x_{\text{op2}}}{r_2}\right) \Omega. \tag{11}$$

The impedance of phase 3 in the power supply circuit:

$$Z_3 = r_3 + jx_3 = \sqrt{r_3^2 + x_{\text{op3}}^2}\angle\varphi_3, \quad \varphi_3 = \arctan\left(\frac{x_{\text{op3}}}{r_3}\right) \Omega. \tag{12}$$

Since the three-phase power supply is symmetrical, therefore, ++ =, and the relationship of each phase voltage can be expressed as:

$$\begin{aligned} U_A &= U_0\angle 0^\circ = U_0, \\ U_B &= U_0\angle -120^\circ = -\frac{U_0}{2} - j\frac{\sqrt{3}}{2}U_0, \\ U_C &= U_0\angle 120^\circ = -\frac{U_0}{2} + j\frac{\sqrt{3}}{2}U_0. \end{aligned} \tag{13}$$

3.2. Calculation of neutral point voltage and current

Figure 3 illustrates a star-connected circuit with unbalanced loads. When the neutral point is open-circuited, nodes *N* and *N*' are no longer equipotential. The node voltage method can be employed to determine the voltage of the load neutral point.

$$\left(\frac{1}{Z_1} + \frac{1}{Z_2} + \frac{1}{Z_3}\right) \times \dot{U}_{N'N} = \frac{\dot{U}_1}{Z_1} + \frac{\dot{U}_2}{Z_2} + \frac{\dot{U}_3}{Z_3}. \tag{14}$$

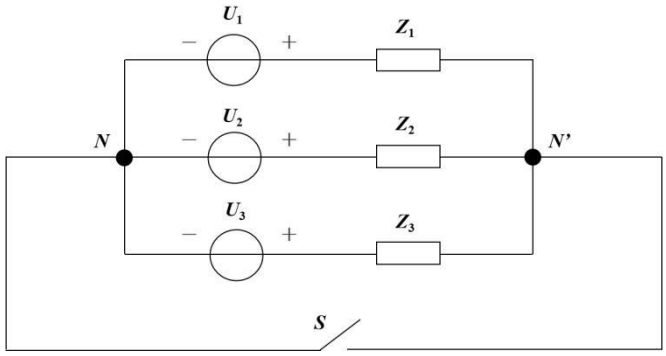


Fig. 3. Three-phase circuit with unbalanced load

Figure 4 shows the voltage relationships under three-phase unbalanced conditions. It can be observed that the voltages at the load terminals of each phase are unequal due to the asymmetry of the three-phase loads. The calculation formulas for the load terminal voltages of each phase are presented as follows.

$$\begin{aligned} \dot{U}_{1^\circ} &= \dot{U}_1 - \dot{U}_{N'N} \\ \dot{U}_{2^\circ} &= \dot{U}_2 - \dot{U}_{N'N} \\ \dot{U}_{3^\circ} &= \dot{U}_3 - \dot{U}_{N'N} \end{aligned} . \tag{15}$$

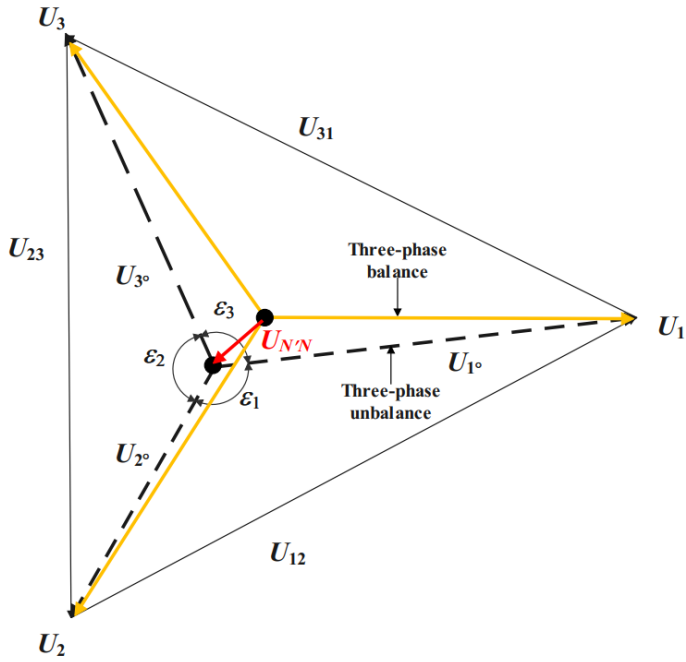


Fig. 4. Relationships among three-phase voltage vectors under unbalanced phase conditions

From $Z_1 = r_1 + jx_{\mathrm{op1}}\ \Omega$, we derive:

$$\frac{1}{Z_1} = \frac{1}{r_1 + jx_1} = \frac{r_1 - jx_1}{(r_1 + jx_1)(r_1 - jx_1)} = \frac{(r_1 - jx_1)}{r_1^2 + x_1^2} = \frac{r_1}{r_1^2 + x_1^2} - j\frac{x_1}{r_1^2 + x_1^2}. \tag{16}$$

Similarly:

$$\frac{1}{Z_2} = \frac{r_2}{r_2^2 + x_2^2} - j\frac{x_2}{r_2^2 + x_2^2}, \quad \frac{1}{Z_3} = \frac{r_3}{r_3^2 + x_3^2} - j\frac{x_3}{r_3^2 + x_3^2}. \tag{17}$$

Accordingly, the sum of the reciprocals of the three-phase impedances can be obtained as:

$$\frac{1}{Z_1} + \frac{1}{Z_2} + \frac{1}{Z_3} = \left(\frac{r_1}{r_1^2 + x_1^2} + \frac{r_2}{r_2^2 + x_2^2} + \frac{r_3}{r_3^2 + x_3^2}\right) - j\left(\frac{x_1}{r_1^2 + x_1^2} + \frac{x_2}{r_2^2 + x_2^2} + \frac{x_3}{r_3^2 + x_3^2}\right). \tag{18}$$

Thus, the three-phase parallel impedance Z_p can be obtained as:

$$Z_P = \frac{1}{\left(\frac{r_1}{r_1^2+x_1^2}+\frac{r_2}{r_2^2+x_2^2}+\frac{r_3}{r_3^2+x_3^2}\right)-j\left(\frac{x_1}{r_1^2+x_1^2}+\frac{x_2}{r_2^2+x_2^2}+\frac{x_3}{r_3^2+x_3^2}\right)}, \tag{19}$$

$$Z_P = \frac{\frac{r_1}{r_1^2+x_1^2}+\frac{r_2}{r_2^2+x_2^2}+\frac{r_3}{r_3^2+x_3^2}}{\left(\frac{r_1}{r_1^2+x_1^2}+\frac{r_2}{r_2^2+x_2^2}+\frac{r_3}{r_3^2+x_3^2}\right)^2+\left(\frac{x_1}{r_1^2+x_1^2}+\frac{x_2}{r_2^2+x_2^2}+\frac{x_3}{r_3^2+x_3^2}\right)^2} + j\frac{\frac{x_1}{r_1^2+x_1^2}+\frac{x_2}{r_2^2+x_2^2}+\frac{x_3}{r_3^2+x_3^2}}{\left(\frac{r_1}{r_1^2+x_1^2}+\frac{r_2}{r_2^2+x_2^2}+\frac{r_3}{r_3^2+x_3^2}\right)^2+\left(\frac{x_1}{r_1^2+x_1^2}+\frac{x_2}{r_2^2+x_2^2}+\frac{x_3}{r_3^2+x_3^2}\right)^2}. \tag{20}$$

Due to the complexity of the calculation formula for the three-phase parallel impedance Z_p, it is assumed for simplicity that:

$$A = \frac{\frac{r_1}{r_1^2+x_1^2}+\frac{r_2}{r_2^2+x_2^2}+\frac{r_3}{r_3^2+x_3^2}}{(\frac{r_1}{r_1^2+x_1^2}+\frac{r_2}{r_2^2+x_2^2}+\frac{r_3}{r_3^2+x_3^2})^2+(\frac{x_1}{r_1^2+x_1^2}+\frac{x_2}{r_2^2+x_2^2}+\frac{x_3}{r_3^2+x_3^2})^2}, \tag{21}$$

$$B = \frac{\frac{x_1}{r_1^2+x_1^2}+\frac{x_2}{r_2^2+x_2^2}+\frac{x_3}{r_3^2+x_3^2}}{(\frac{r_1}{r_1^2+x_1^2}+\frac{r_2}{r_2^2+x_2^2}+\frac{r_3}{r_3^2+x_3^2})^2+(\frac{x_1}{r_1^2+x_1^2}+\frac{x_2}{r_2^2+x_2^2}+\frac{x_3}{r_3^2+x_3^2})^2}. \tag{22}$$

Therefore, the three-phase parallel impedance Z_p can be simplified as:

$$Z_P = A + jB, \tag{23}$$

$$\frac{\dot{U}_1}{Z_1} = \frac{U_0\angle 0^\circ}{r_1+jx_1} = \frac{U_0}{r_1+jx_1} = \frac{U_0 r_1}{r_1^2+x_1^2} - j\frac{U_0 x_1}{r_1^2+x_1^2}, \tag{24}$$

$$\frac{\dot{U}_2}{Z_2} = \frac{U_0\angle -120^\circ}{r_2+jx_2} = \frac{-\frac{U_0}{2}-j\frac{\sqrt{3}}{2}U_0}{r_2+jx_2} = -\frac{\frac{U_0 r_2}{2}+\frac{\sqrt{3}U_0 x_2}{2}}{r_2^2+x_2^2} + j\frac{\frac{U_0 x_2}{2}-\frac{\sqrt{3}U_0 r_2}{2}}{r_2^2+x_2^2}, \tag{25}$$

$$\frac{\dot{U}_3}{Z_3} = \frac{U_0\angle 120^\circ}{r_3+jx_3} = \frac{-\frac{U_0}{2}+j\frac{\sqrt{3}}{2}U_0}{r_3+jx_3} = \frac{\frac{\sqrt{3}U_0 x_3}{2}-\frac{U_0 r_3}{2}}{r_3^2+x_3^2} + j\frac{\frac{U_0 x_3}{2}+\frac{\sqrt{3}U_0 r_3}{2}}{r_3^2+x_3^2}. \tag{26}$$

The three-phase neutral point voltage refers to the potential difference between the neutral point (N) and the reference ground (or the power supply neutral point) in a three-phase star connection, and its magnitude is determined by the degree of balance of the three-phase load and voltage.

$$\begin{aligned}\dot{I}_{N'N} = \frac{\dot{U}_1}{Z_1} + \frac{\dot{U}_2}{Z_2} + \frac{\dot{U}_3}{Z_3} = \frac{U_0 r_1}{r_1^2 + x_1^2} - j\frac{U_0 x_1}{r_1^2 + x_1^2} - \frac{\frac{U_0 r_2}{2} + \frac{\sqrt{3}U_0 x_2}{2}}{r_2^2 + x_2^2} \\ + j\frac{\frac{U_0 x_2}{2} - \frac{\sqrt{3}U_0 r_2}{2}}{r_2^2 + x_2^2} + \frac{\frac{\sqrt{3}U_0 x_3}{2} - \frac{U_0 r_3}{2}}{r_3^2 + x_3^2} + j\frac{\frac{U_0 x_3}{2} + \frac{\sqrt{3}U_0 r_3}{2}}{r_3^2 + x_3^2}.\end{aligned} \tag{27}$$

Given the considerable complexity of the aforementioned formula, a simplified treatment is appropriate.

$$C = \frac{U_0 r_1}{r_1^2 + x_1^2} - \frac{\frac{U_0 r_2}{2} + \frac{\sqrt{3}U_0 x_2}{2}}{r_2^2 + x_2^2} + \frac{\frac{\sqrt{3}U_0 x_3}{2} - \frac{U_0 r_3}{2}}{r_3^2 + x_3^2}, \tag{28}$$

$$D = -\frac{U_0 x_1}{r_1^2 + x_1^2} + \frac{\frac{U_0 x_2}{2} - \frac{\sqrt{3}U_0 r_2}{2}}{r_2^2 + x_2^2} + \frac{\frac{U_0 x_3}{2} + \frac{\sqrt{3}U_0 r_3}{2}}{r_3^2 + x_3^2}. \tag{29}$$

According to Eqs. (27)–(29), the neutral point current $I_{N'N}$ can be obtained as:

$$\dot{I}_{N'N} = C + jD. \tag{30}$$

The neutral point voltage $U_{N'N}$ refers to the potential difference between the neutral point of a polyphase system (such as a three-phase star connection) and the reference ground, and its magnitude is determined by the degree of balance in the phase voltages and loads. Specifically, it equals the product of the three-phase parallel resistance and the neutral point current.

$$\dot{U}_{N'N} = \dot{I}_{N'N} \times Z_P = (A + jB) \times (C + jD) = (ACBD) + j(BC + AD). \tag{31}$$

3.3. Calculation of load voltage and current

Based on the circuit diagram presented in Fig. 2, it can be established that the voltage applied to the load is precisely the resultant of subtracting the neutral point voltage from the respective phase input voltage. Therefore, the load voltage for each phase can be calculated as shown in Eqs. (32)–(34) respectively.

$$\dot{U}_{1^\circ} = \dot{U}_1 - \dot{U}_{N'N} = U_0 \angle 0^\circ - \dot{U}_{N'N} = (U_0 - AC + BD) - j(BC + AD), \tag{32}$$

$$\dot{U}_{2^\circ} = \dot{U}_2 - \dot{U}_{N'N} = U_0 \angle -120^\circ - \dot{U}_{N'N} = \left(-\frac{U_0}{2} - AC + BD\right) - j\left(\frac{\sqrt{3}U_0}{2} + BC + AD\right), \tag{33}$$

$$\dot{U}_{3^\circ} = \dot{U}_3 - \dot{U}_{N'N} = U_0 \angle 120^\circ - \dot{U}_{N'N} = \left(-\frac{U_0}{2} - AC + BD\right) + j\left(\frac{\sqrt{3}U_0}{2} - BC - AD\right). \tag{34}$$

Subsequently, the per-phase currents I_1, I_2 and I_3 are obtained as expressed in Eqs. (35)–(37), respectively.

$$I_1 = \frac{\dot{U}_{1^\circ}}{Z_1} = \frac{U_{1^\circ}}{\sqrt{r_1^2 + x_1^2}} = \frac{\sqrt{(U_0 - AC + BD)^2 + (BC + AD)^2}}{\sqrt{r_1^2 + x_1^2}}, \tag{35}$$

$$I_2 = \frac{\dot{U}_{2^\circ}}{Z_2} = \frac{U_{2^\circ}}{\sqrt{r_2^2 + x_2^2}} = \frac{\sqrt{\left(-\frac{U_0}{2} - AC + BD\right)^2 + \left(\frac{\sqrt{3}U_0}{2} + BC + AD\right)^2}}{\sqrt{r_2^2 + x_2^2}}, \tag{36}$$

$$I_3 = \frac{\dot{U}_{3^\circ}}{Z_3} = \frac{U_{3^\circ}}{\sqrt{r_3^2 + x_3^2}} = \frac{\sqrt{\left(-\frac{U_0}{2} - AC + BD\right)^2 + \left(\frac{\sqrt{3}U_0}{2} - BC - AD\right)^2}}{\sqrt{r_3^2 + x_3^2}}. \tag{37}$$

During the smelting process in an EAF, electrode positions are typically adjusted dynamically based on the target arc length to maintain consistent three-phase impedance, thereby mitigating three-phase unbalance. Therefore, under normal operating conditions, an EAF is generally equipped with an electrode control system. This system mainly installs Rogowski coils at the output terminals of the EAF transformer to dynamically measure the voltage and current on the low-voltage side of the transformer, so as to obtain three-phase impedance values. For this reason, it is necessary to calculate the voltage and impedance on the low-voltage side of the EAF transformer. In the secondary circuit of the EAF power supply system, the input voltage is transmitted through impedance components including the EAF transformer and reactor. Therefore, when calculating the voltage at the output terminal of the EAF transformer, the inherent voltage drops of the transformer and reactor must be excluded.

As shown in Fig. 2, the combined reactance of the EAF transformer and reactor is given by:

$$x_{s1} = x_{\text{reactor1}} + x_{\text{transformer1}}, \tag{38}$$

$$r_{s1} = r_{\text{reactor1}} + r_{\text{transformer1}}, \tag{39}$$

$$z_{s1} = \sqrt{x_{s1}^2 + r_{s1}^2}. \tag{40}$$

In which: x_{s1} denotes the total reactance of the transformer and reactor of phase 1, Ω; r_{s1} denotes the total resistance of the transformer and reactor of phase 1, Ω; z_{s1} denotes the total impedance of the transformer and reactor of phase 1, Ω.

Based on the resistance and reactance values of the transformer and reactor, the power factor angle φ_{s1} is obtained.

$$\varphi_{s1} = \arctan\left(\frac{x_{s1}}{r_{s1}}\right). \tag{41}$$

Hence, the voltage drop U_{s1} resulting from the transformer and reactor can be expressed as:

$$U_{s1} = I_1 \times \sqrt{x_{s1}^2 + r_{s1}^2}. \tag{42}$$

The resistance and reactance on the low-voltage side of the EAF transformer are attributed to the secondary circuit and the electric arc. Hence, the total resistance of the secondary circuit and arc for one phase is $r_{L1} = r_{\text{circuit1}} + r_{\text{arc1}}$, while the total reactance of the secondary circuit for one phase is x_{L1}. Accordingly, the power factor angle φ_{L1} on the low-voltage side for one phase can be calculated as:

$$\varphi_{L1} = \arctan\left(\frac{x_{L1}}{r_{L1}}\right). \tag{43}$$

According to the research conducted by Cao, the load voltage U_{1^*} on the low-voltage side of phase 1 can be calculated as:

$$U_{1^*} = \sqrt{U_0^2 - [U_{s1}\sin(\varphi_{s1} - \varphi_{L1})]^2} - U_{s1}\cos(\varphi_{s1} - \varphi_{L1}). \tag{44}$$

By the same principle, the low-voltage side load voltages for phases 2 and 3, denoted U_{2^*} and U_{3^*} are determined.

$$U_{2^*} = \sqrt{U_0^2 - [U_{s2}\sin(\varphi_{s2} - \varphi_{L2})]^2} - U_{s2}\cos(\varphi_{s2} - \varphi_{L2}), \tag{45}$$

$$U_{3^*} = \sqrt{U_0^2 - [U_{s3}\sin(\varphi_{s3} - \varphi_{L3})]^2} - U_{s3}\cos(\varphi_{s3} - \varphi_{L3}). \tag{46}$$

3.4. Calculation of power supply parameters

Based on the calculated results of the three-phase currents, the power supply parameters for each phase circuit are obtained as follows:

Active power of phase 1 at the input terminals of the transformer, denoted as P_{h1}:

$$P_{h1} = I_1^2 \times r_1. \tag{47}$$

Similarly, the active power for phase 2 and phase 3 at the input terminals of the transformer can be obtained, denoted as P_{h2} and P_{h3}.

$$P_{h2} = I_2^2 \times r_2, \tag{48}$$

$$P_{h3} = I_3^2 \times r_3. \tag{49}$$

In an analogous way, based on the power supply circuit of the EAF, the calculation results of the three-phase apparent power S_{h1}, S_{h2} and S_{h3} can also be obtained:

$$S_{h1} = I_1^2 \times z_1, \tag{50}$$

$$S_{h2} = I_2^2 \times z_2, \tag{51}$$

$$S_{h3} = I_3^2 \times z_3. \tag{52}$$

According to Eqs. (47)–(52), the power factor of each phase can be obtained, as shown in Eq. (53).

$$\cos\phi_1 = P_{h1}/S_{h1}, \quad \cos\phi_2 = P_{h2}/S_{h2}, \quad \cos\phi_3 = P_{h3}/S_{h3}. \tag{53}$$

Similarly, the active power at the outgoing terminal of the transformer can be determined accordingly, and P_{L1}, P_{L2}, P_{L3} represent the three-phase power at the output terminals of the transformer, respectively.

$$P_{L1} = I_1^2 \times r_{L1}, \tag{54}$$

$$P_{L2} = I_2^2 \times r_{L2}, \tag{55}$$

$$P_{L3} = I_3^2 \times r_{L3}. \tag{56}$$

In the above equation, r_{L1}, r_{L2} and r_{L3} denote the resistances of phase 1, phase 2 and phase 3 at the outgoing terminals of the transformer, respectively.

4. Simulation results for the influence of three-phase impedance unbalance on power quality

Taking a 120 t EAF (EAF) as an example, the equipment parameters of its power supply circuit are listed in Table 2. According to the table, the EAF transformer is designed with a capacity of 120 MVA and a hot heel of 80 t. Thanks to efficient scrap preheating and continuous flat-bath smelting, the tap-to-tap time approaches 30 min. On the primary side, the input voltage of EAF transformer is 35 kV. On the secondary side, the maximum output voltage is 1165 V, with sixteen adjustable steps each of 30 V. The transformer features a short-circuit impedance of 6.47% and

Table 2. Basic parameters of EAF and medium-voltage equipment

System components	Parameters	Units	Values
EAF	**Furnace capacity**	t	120
	Hot heel	t	80
	Diameter of shell	mm	6 500
	Tap-to-tap time	min	30
	Electricity consumption per ton of steel	kWh/t	330
	Electrode consumption per ton of steel	kg/t	0.8
Transformer	Transformer capacity	MVA	120
	Overload capacity	%	20
	Short-circuit impedance	%	6.47%
	Primary voltage	kV	35
	Secondary voltage	V	1 165–1 045–715
	Number of taps		16
	Voltage range of the constant-power stage	V	1 165–1 045
	Maximum secondary current	A	66 299
Reactor	Reactor capacity	kvar	14 000
	Number of taps		6
	Impedance percentage	%	100, 80, 60, 40, 20, 0
	Rated current	A	2 183
Secondary circuit	Impedance of secondary circuit	mΩ	$0.3 + j2.8$

a maximum rated secondary current of 66 299 A. The reactor is designed with a rated capacity of 14 000 kvar and a rated current of 2 183 A, and its tap configuration comprises six steps. Moreover, the secondary-circuit impedance of the EAF power supply is measured as $0.3 + j2.8$ mΩ.

Figure 5 shows the simulation influence of the three-phase impedance unbalance degree on the neutral point voltage and the three-phase voltage unbalance. It can be seen from the figure that as the impedance unbalance degree increases, both the neutral point voltage and the three-phase voltage unbalance increase significantly. Under impedance unbalance levels of 10%, 20% and 30%, the neutral-point voltage attains 17.44 V, 35.01 V and 52.84 V, respectively, which in turn leads to three-phase voltage unbalance degrees of 5.00%, 10.04% and 15.13%. For a 5% three-phase impedance unbalance degree, the current difference between phase 1 and phase 3 within the EAF's supply circuit is 1 554 A. As the impedance unbalance degree increases to 30%, this current difference becomes 9 384 A, accompanied by an increase in the current unbalance degree from 2.50% to 14.96%. The three-phase impedance unbalance in EAF leads to differences in arc length among phases. The arc in the high-impedance phase is compressed and shortened, while that in the low-impedance phase is elongated, which can be seen from Fig. 6. This simulation results in an uneven temperature distribution within the molten bath, forming local overheating or underheating zones, which impairs the uniformity of chemical reactions, reduces smelting efficiency, and exacerbates the wear of both the furnace lining and the electrical equipment.

Figure 7 demonstrates the simulation impact of the impedance unbalance degree on the three-phase arc length. As is evident from the figure, a notable increase in the differences among the three-phase arc length occurs as the impedance unbalance degree increases. As the impedance unbalance degree increases from 5% to 30%, the three-phase arc length difference rises from 13 mm

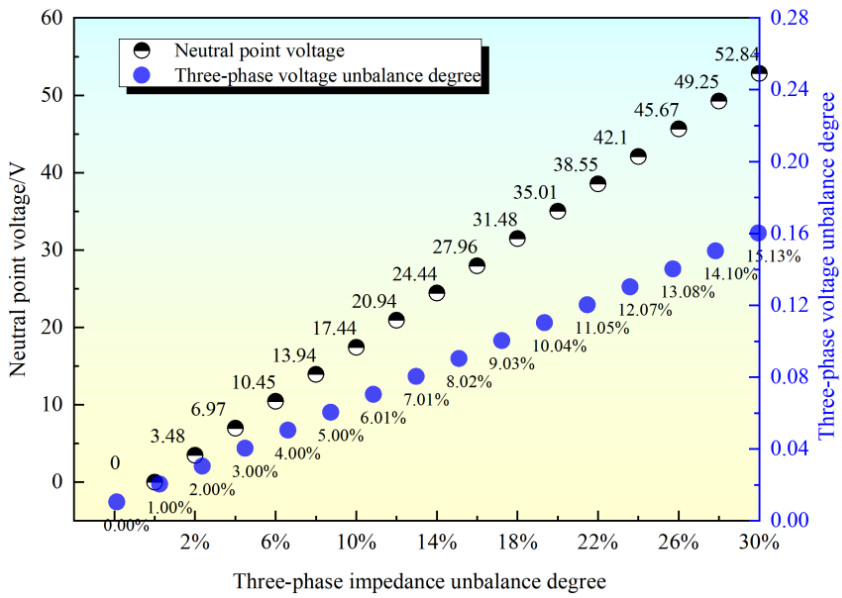


Fig. 5. Simulation results for the influence of impedance unbalance degree on neutral-point voltage and three-phase voltage unbalance

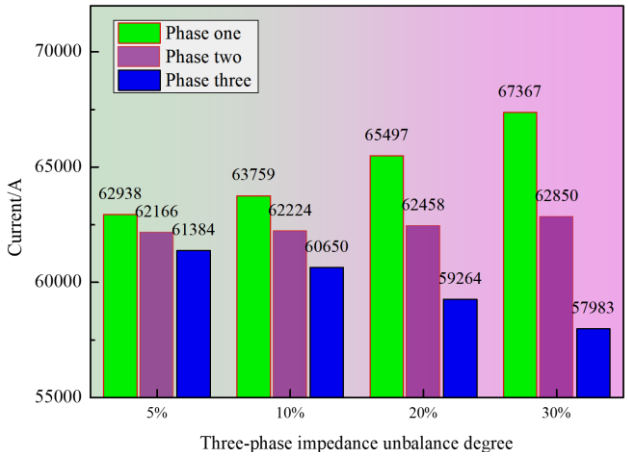


Fig. 6. Simulation results for the effect of three-phase impedance unbalance on current unbalance

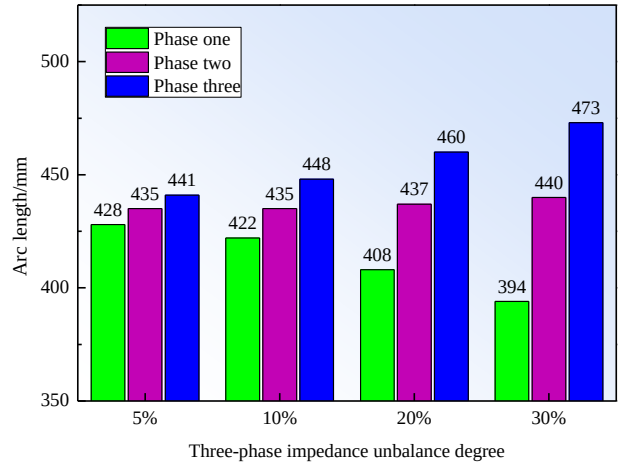


Fig. 7. Simulation results for the effect of three-phase impedance unbalance on arc length

to 79 mm. A significant deviation in three-phase arc length subsequently results in three-phase power unbalance, uneven heating of the molten pool, unstable smelting temperature, frequent electrode adjustments, increased power consumption, and localized erosion damage to the furnace lining.

Due to three-phase unbalance, negative-sequence current arises from the EAF smelting process. Negative-sequence current causes reverse deflection of the electric arc, disrupts the thermally symmetric distribution inside the furnace, and consequently reduces smelting efficiency while accelerating the wear of electrodes and lining. For every 1% increase in negative-sequence current, the electricity consumption per ton of steel rises by approximately 0.5% to 1.5%. Three-phase impedance unbalance generates zero-sequence current, which induces arc fluctuation and unbalance, degrades power supply quality, intensifies equipment heating losses, disturbs electrode regulation, and reduces the stability of smelting conditions.

In the course of the EAF smelting operation, the three-phase currents are designated respectively as I_1, I_2 and I_3. The expressions for the positive-sequence current I_a and the negative-sequence current I_b are respectively given as follows:

$$I_a = \frac{1}{3} \times (I_1 + a \times I_2 + a^2 \times I_3), \tag{57}$$

$$I_b = \frac{1}{3} \times (I_1 + a^2 \times I_2 + a \times I_3), \tag{58}$$

in which,
$$a = e^{j120^\circ} = -\frac{1}{2} + j\frac{\sqrt{3}}{2}, \quad a^2 = e^{j240^\circ} = -\frac{1}{2} - j\frac{\sqrt{3}}{2}. \tag{59}$$

In EAF melting, the ratio of the negative-sequence current to the positive-sequence current (I_b/I_a) is a core indicator for measuring the degree of three-phase unbalance, and under the condition of a fixed short-circuit capacity, it directly determines the voltage unbalance factor. GB50056-93 Design Code for Electric Heating Equipment Installations mandates that the voltage unbalance degree introduced by an EAF shall not exceed 1.3% under normal conditions and 2.6% under short-term conditions. The degree of voltage unbalance at the point of common coupling (PCC) is expressed as the ratio of the negative-sequence voltage to the positive-sequence voltage. Under the condition that the short-circuit capacity S_{Sc} at the PCC and the input voltage U_N ε_U is derived as follows:

$$\varepsilon_U = \frac{S_{Sc} \times I_b}{\sqrt{3} U_N} \times 100\%. \tag{60}$$

The simulation results of three-phase impedance unbalance on both the negative-sequence current and the voltage unbalance at the point of common coupling is depicted in Fig. 8. From this figure, it is evident that an increase in impedance unbalance leads to a pronounced increase in both the negative-sequence current and the voltage unbalance. At impedance unbalance degrees of 10%, 20% and 30%, the negative-sequence current reaches 2.89%, 5.80% and 8.76%, respectively. While the corresponding voltage unbalance degrees are 0.276%, 0.556% and 0.846%, respectively. Consequently, during EAF smelting, it is of great significance to stably control the three-phase unbalance degree for the efficient smelting and safe operation of the furnace.

To verify the accuracy of the developed model, a 128 t Quantum EAF from a steel plant is adopted as the research object. Developed by Primetals Technologies, this EAF is equipped with a scrap preheating system, enabling large heel-metal operation and full-process submerged-arc foaming-slag smelting. The furnace is furnished with a 120 MVA transformer and a 14 000 kvar reactor, and the secondary circuit impedance is $0.3 + j2.8$ mΩ. Voltage and current transformers installed on the high-voltage side are utilized to acquire electrical parameters at the input side, including three-phase voltage, current, power and power factor. At the transformer outlet terminal, Rogowski coils coupled with the matched electrode regulation control system are employed to obtain output-side parameters such as voltage, current, power and impedance. More than 20 sets of valid industrial smelting data were collected during on-site measurements, among which two sets are selected for the calibration and validation of the established mathematical model. Figure 9 presents the comparison between model-predicted results and actual industrial data. It can be observed that the model-predicted results are in good agreement with the actual industrial data. The minor discrepancies are mainly attributed to the difficulty in accurately predicting the operating reactance coefficients k_1, k_2 and k_3.

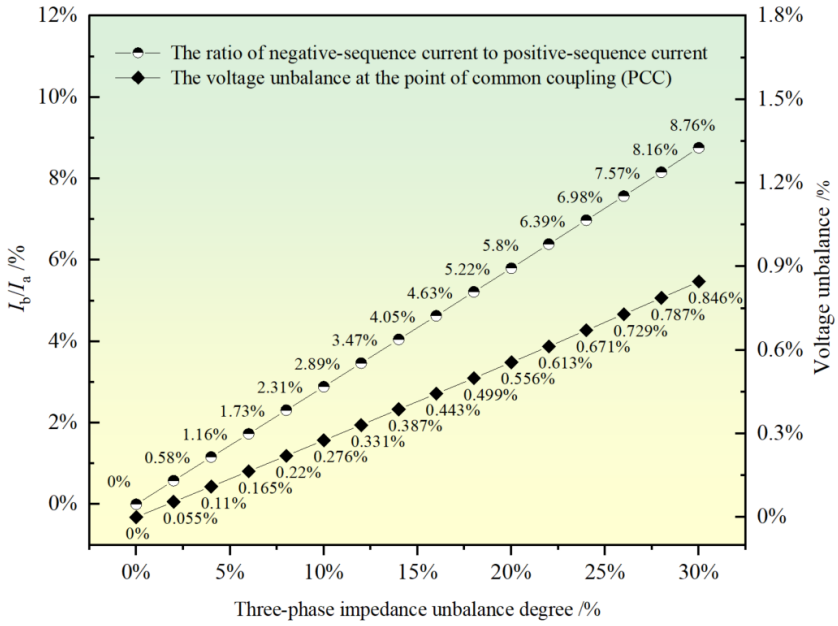


Fig. 8. Simulation results for effects of impedance unbalance degree on negative-sequence current and voltage unbalance

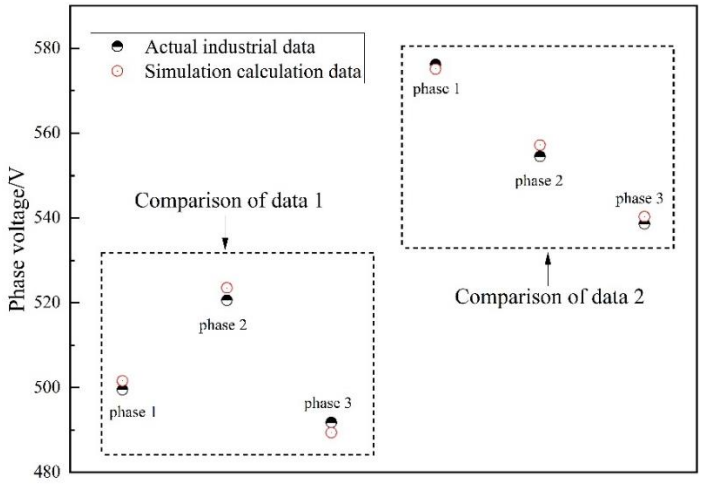


Fig. 9. Comparison between model calculations and industrial data

5. Conclusion

In EAF smelting operations, the unbalanced characteristics of three-phase loads are critical factors affecting electrical energy losses, molten bath temperature uniformity, and smelting efficiency. To address this issue, this paper establishes a mathematical model for key parameters

that influence the production stability of EAFs based on a three-phase unbalanced circuit. These parameters include neutral point voltage, three-phase voltage unbalance degree, three-phase current, arc length, negative-sequence current, and voltage unbalance degree at the point of common coupling (PCC). Simulation analysis conducted on a 120 t EAF reveals that as the degree of impedance unbalance increases, both the neutral point voltage and the three-phase voltage unbalance degree exhibit an upward trend, while the inter-phase current difference and current unbalance degree also increase significantly. Notably, when the impedance unbalance degree rises from 10% to 30%, the three-phase arc length difference expands from 26 mm to 79 mm, the relative negative-sequence current increases from 2.89% to 8.76%, and the PCC voltage unbalance degree also rises from 0.276% to 0.846%.

Acknowledgements

The authors acknowledge the support of the Guangdong Provincial Key Area Research and Development Program (No. 2025B0101020002) for this paper.

References

[1] Olczykowski Z., *Electric Arc Furnaces as a Cause of Current and Voltage Asymmetry*, Energies, vol. 14, no. 16, 5058 (2021), DOI: 10.3390/en14165058.

[2] Hocine L., Yacine D., Kamel B., Samira K.M., *Improvement of electrical arc furnace operation with an appropriate model*, Energy, vol. 34, no. 9, pp. 1207–1214 (2009), DOI: 10.1016/j.energy.2009.03.003.

[3] Beites L.F., Mayordomo J.G., Hernandez A., Asensi R., *Harmonics, interharmonics and unbalances of arc furnaces: a new frequency domain approach*, 8th International Conference on Harmonics and Quality of Power Proceedings (1998), DOI: 10.1109/ICHQP.1998.760188.

[4] Jaipradidtham, Chamni, *A control of real voltage and harmonic analysis with adaptive static var of EAF for power quality improvement by Grey Markov method*, 2016 IEEE 6th International Conference on Power Systems (2016), DOI: 10.1109/ICPS.2016.7584250.

[5] Aliferov A.I., Goreva L.P., Bikeev R.A., *Operational asymmetry of the secondary conductor in an ultra-high-power electric arc furnace*, Russian Electrical Engineering, vol. 96, no. 7, pp. 503–509, DOI: 10.3103/S1068371225700658.

[6] Kozyra J., Lozynskyy A., Łukasik Z., Kuśmińska-Fijałkowska A., Kutsyk A., Kasha K., *Increasing the level of autonomy of control of the EAF by Weakening Interphase Interactions*, Energies, vol. 16, no. 24, 8114 (2025), DOI: 10.3390/en16248114.

[7] Dong Y., *Research on loss in power grid induced by three-phase imbalance*, Journal Electrical and Electronic Engineering, vol. 8, no. 3, pp. 103–108 (2020), DOI: 10.11648/J.JEEE.20200803.14.

[8] Diao G.X., Guanxun D., Ni H., Si W., Gu Y., Yang J., *Multi-physics numerical research in oil-immersed three-phase transformer under load unbalance*, Energies, vol. 18, no. 5, pp. 1217–1250 (2025), DOI: 10.1016/j.energy.2009.03.003.

[9] Gala M., Sawicki A., Jagiela K., *Modeling of asymmetrical operating states of AC electric arc furnace in the power system*, IEEE 20th International Conference on Computational Problems of Electrical Engineering (2019), DOI: 10.1109/CPEE47179.2019.8949094.

[10] Sivtsov A.V., Sheshukov O.Y., Tsymbalist M.M., Nekrasov I.V., Makhnutin A.V., *Steel Semiproduct Melting Intensification in EAFs Using Coordinated Control of Electric and Gas Conditions: I. Heat Exchange and Structure of the EAF Laboratory*, Russian Metallurgy (Metally), no. 6, pp. 656–569 (2019).

[11] Shurgin A.U., Kornilov G.P. *et al*. *Symmetry of Arc Furnace Operation*, Steel in Translation, vol. 47, no. 11, pp. 732–736 (2017).

[12] Babaei Z., Samet H., *Vector polynomial Electric Arc Furnace models*, IEEE Transactions on Power Delivery, vol. 40, no. 3, pp. 1694–170 (2025), DOI: 10.1109/TPWRD.2025.3559806.